

Carbon Monoxide Stripe Motion Driven by Correlated Lateral Hopping in a 1.4×1.4 Monolayer Phase on Cu(111)

Nana K. M. Nazriq, Peter Krüger, and Toyo Kazu Yamada*

Cite This: *J. Phys. Chem. Lett.* 2020, 11, 1753–1761

Read Online

ACCESS |

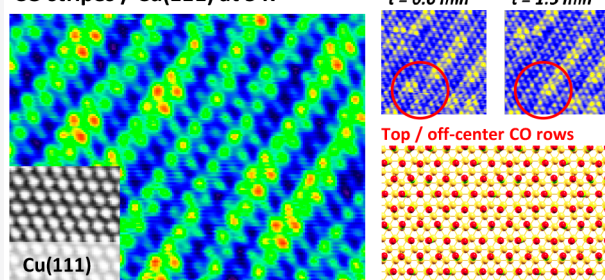
Metrics & More

Article Recommendations

Supporting Information

ABSTRACT: We report an ultra-high-vacuum low-temperature (4.6 K) scanning tunneling microscopy study of the molecular structure and dynamics of a carbon monoxide (CO) monolayer adsorbed at 20 K on Cu(111). We observe the well-known 1.4×1.4 phase of CO/Cu(111) for the first time in real-space imaging. At 4.6 K, the hexagonal symmetry of the monolayer is locally broken by the formation of stripes made of single and double CO rows of different apparent heights. Using density functional theory calculations, we assign the high rows to CO molecules adsorbed mostly at off-center top sites and the low rows to bridge sites. Groups of three or four very high molecules appear randomly and are assigned to nearest-neighbor, titled top site molecules. We observe simultaneous hopping of a few CO molecules between adjacent top and bridge sites, which produces the apparent motion of the stripe pattern.

CO stripes / Cu(111) at 5 K



The adsorption of carbon monoxide (CO) has been studied extensively in the past several decades because a precise understanding of the structure formation and adsorption site on metal surfaces is an important key for unveiling catalysis and molecular surface interaction.^{1–3} More recently, greatly diverse research on CO was conducted. Single CO molecules adsorbed on noble metal substrates at cryogenic temperatures under ultrahigh vacuum (UHV) conditions are used as a standard sample to demonstrate single-molecule manipulation^{4,5} and also as a building block to produce artificial graphene nanoribbon molecules⁶ or kagome lattices with exotic electronic properties of a higher-order topological insulator.^{7–10} CO adsorbed on different substrates can form monolayers with a variety of lattice structures.^{11–16} For the extensively studied CO/Cu(111) system,^{17–30} several apparently simple monolayer structures (such as 1.4×1.4) are readily observed via low-energy electron diffraction (LEED) but have never been confirmed using a real-space imaging technique. Here, we solve this puzzle that has lasted for decades.

CO adsorbs preferentially at the top site of Cu(111). Kole et al. measured the potential energy surface of CO at low coverage on Cu(111) at 170–210 K using helium spin-echo spectroscopy.²⁶ The top adsorption site was found to be the most stable, followed by the bridge site (38 meV), while the hollow site is a local maximum of the potential energy surface and thus unstable. For CO/Cu(111), various monolayer phases have been found.^{17–30} At an adsorption temperature of 85 K, CO forms a $(\sqrt{3} \times \sqrt{3})R30$ structure, with a saturation coverage of $\Theta = 0.33$, where one of three top sites is occupied.^{24,25,31} Below 80 K, several denser phases have been

observed by LEED, including 1.5×1.5 R18 ($\Theta = 0.44$)²⁵ and 1.4×1.4 ($\Theta = 0.51$).¹⁸ In these cases, CO molecules adsorb not only at top sites but also at bridge sites,^{19,28,29} but adsorption at hollow sites is unlikely.²⁶ Reflection adsorption infrared spectroscopy (RAIRS) results obtained for the CO/Cu(111) surface at approximately 15 K indicate that all CO chemisorbs at top sites up to a coverage of $\Theta = 0.33$, while bridge sites also become occupied for higher coverages.²⁷ In the adsorption temperature regime of 7–77 K, the ratio of bridge to top sites strongly increases with coverage such that at $\Theta = 0.5$ there are approximately as many bridge as top sites.²⁷ Surprisingly, real-space evidence for the dense phases of CO/Cu(111) is scarce. The only scanning tunneling microscopy (STM) results for coverages $\Theta > 0.4$ were reported by Bartels et al.,³¹ who observed a dense monolayer at 15 K with a $p(4 \times 4)$ periodicity. They proposed a model of four top and five bridge site CO molecules in the 4×4 cell, corresponding to $\Theta = 0.56$ and an approximate 1.33×1.33 periodicity, which is clearly different from those of the structures identified by LEED. Considering the tremendous progress in STM imaging over the past several decades and the role of CO/Cu(111) as a prototype system of surface science, it is most surprising that the molecular structure of well-established low-temperature phases, especially 1.4×1.4 , has not been revealed to date.

Received: December 10, 2019

Accepted: February 9, 2020

Published: February 9, 2020

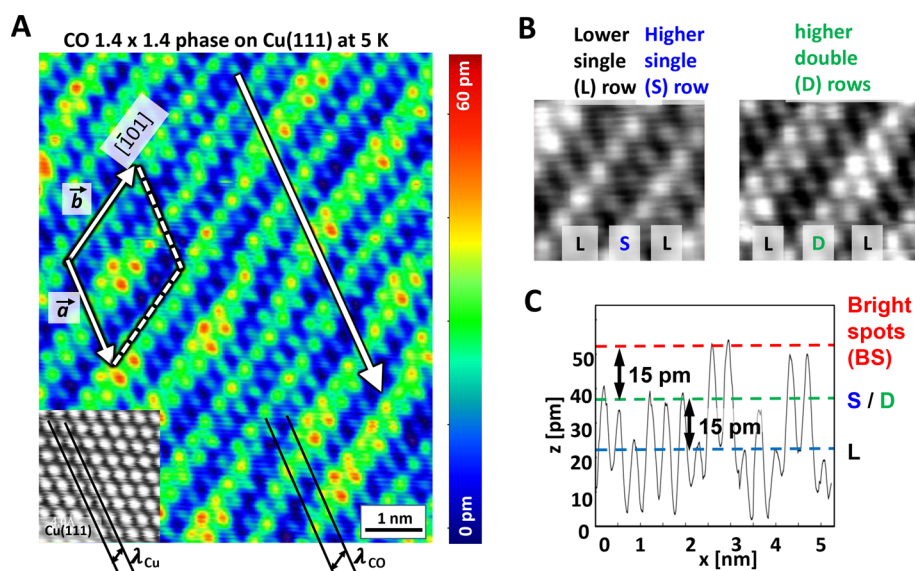


Figure 1. UHV STM study on the 1.4×1.4 CO monolayer film on Cu(111) at 4.6 K with a CO-terminated W tip. (A) STM topographic image ($7 \text{ nm} \times 8.6 \text{ nm}$; $V_s = 40 \text{ mV}$; $I = 0.73 \text{ nA}$). The inset represents an STM image corresponding to underlying fcc Cu(111) atoms. \vec{a} and \vec{b} denote a 5×5 CO molecule unit cell of the 1.4×1.4 phase corresponding to a 7×7 cell of the Cu(111) substrate. (B) Enlarged STM images ($2 \text{ nm} \times 1.9 \text{ nm}$) taken from panel A. The stripes along \vec{a} are lower CO rows (L) alternating with either single (S) or double (D) higher rows. (C) Height profile along the white arrow in panel A.

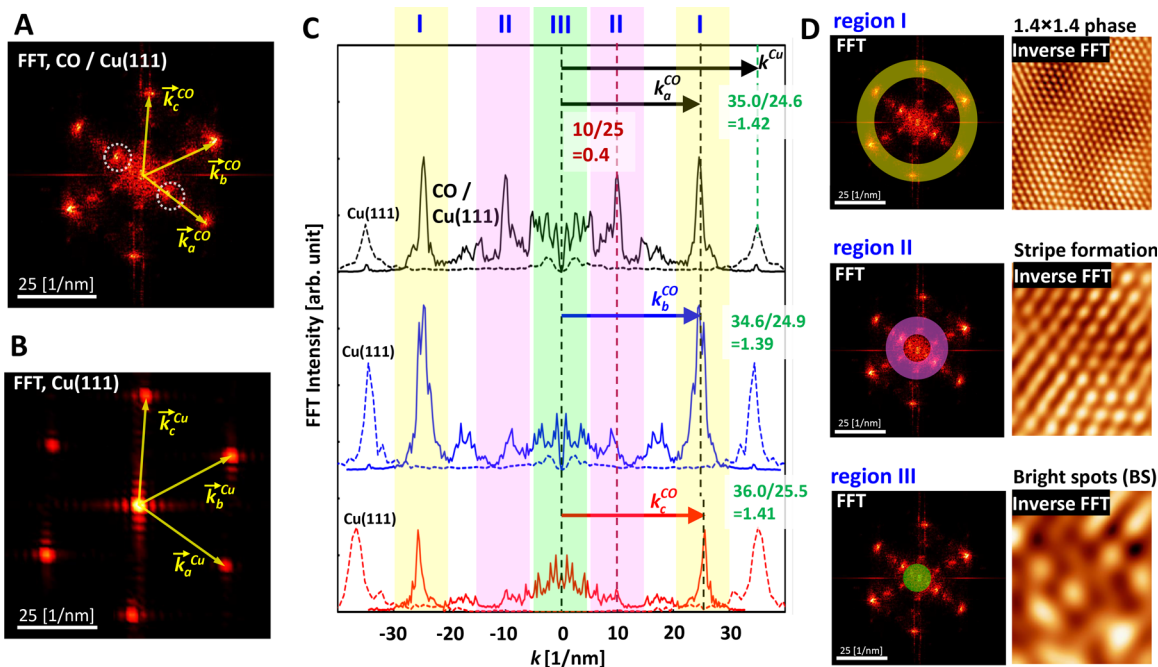


Figure 2. (A) Fourier transform (FFT) image obtained from Figure 1A. Six symmetric spots are observed. Reciprocal lattice vectors \vec{k}_a^{CO} and \vec{k}_b^{CO} correspond to $2\pi/(\vec{a}/5)$ and $2\pi/(\vec{b}/5)$, respectively, and $\vec{k}_c^{\text{CO}} = \vec{k}_b^{\text{CO}} - \vec{k}_a^{\text{CO}}$ is shown. (B) FFT image of the clean Cu(111) substrate. (C) Three line profiles along \vec{k}_a^{CO} (black), \vec{k}_b^{CO} (blue), and \vec{k}_c^{CO} (red) in panel A. The line profile along \vec{k}_a^{Cu} obtained from panel B is also shown as a dotted black line. Regions I–III denote the main peaks, submain peaks, and Γ point regions, respectively. (D) Inverse FFT images obtained from regions I–III in the FFT image obtained on the CO surface.

Here we report the first real-space observation of the 1.4×1.4 phase of CO/Cu(111) using STM experiments performed at 4.6 K under UHV. The CO monolayer was grown on an atomically flat and clean Cu(111) surface held at approximately 20 K. The STM analysis provides detailed insight into the local arrangement of the CO molecules, which complements the lattice information obtained by LEED.^{19,28} Significantly, we observe that the CO monolayer consists of

dense CO rows, made of higher single and double (S and D, respectively) rows alternating with lower (L) rows. This leads to a one-dimensional, quasi-periodic patterning of the STM contrast, i.e., the formation of stripes with an average width of 2.5 CO rows as clearly established by Fourier analysis. From the STM contrast and STM spectroscopy dI/dV measurements, the L rows are attributed to CO molecules adsorbed on Cu(111) bridge sites and the S and D rows to molecules

adsorbed on mostly off-center top sites. The higher D rows are not uniform but contain clusters of three or four CO molecules [named bright spots (BS)] that appear to be significantly higher (+15 pm). By comparison with CO/Cu(100),^{32,33} these clusters can be attributed to tilted CO molecules on nearest-neighbor top sites. The stripe patterning is nonperiodic, and D rows frequently evolve into S rows (and vice versa) along the row direction.

The time evolution of the CO monolayer is studied by taking STM images at 1.5 min intervals. The connection point between some single and double rows is found to move between images. This leads to an apparent, one-dimensional wave motion of the stripe pattern and is explained as a correlated hopping of several CO molecules from bridge to top sites in the direction perpendicular to the rows.

STM on the 1.4×1.4 CO Phase. We adsorbed CO on the Cu(111) substrate at approximately 20 K and carefully monitored the overlayer structure as a function of the amount of CO. At a CO dosage of 0.1 L, only randomly distributed single molecules are found (see Figure S1A and ref 18). At a dose of 0.5 L, the well-known ($\sqrt{3} \times \sqrt{3}$) R30° phase appears and covers ~50% of the surface, while the rest of the surface shows disordered CO structures. A drastic change occurs at 1.0 L, when the whole surface is covered by a dense, ordered CO monolayer. Figure 1A shows an STM image of this monolayer, obtained with a CO-functionalized W tip under UHV at 4.6 K. Each bright spot corresponds to a single CO molecule. The inset (bottom left corner) in Figure 1A shows the atomic image of the underlying Cu(111) substrate. The lattice constant ratio between CO and Cu is very nearly $7/5 = 1.4$ along all three axes of the hexagonal lattice, such that the CO layer can clearly be identified as the 1.4×1.4 phase, which had previously been observed only by LEED.¹⁸ The commensurate 1.4×1.4 phase corresponds to a supercell with unit vectors \vec{a} and \vec{b} shown in Figure 1A, along the [01 $\bar{1}$] and [$\bar{1}$ 01] directions of fcc Cu, respectively. The supercell consists of 7×7 Cu surface cells and contains $5 \times 5 = 25$ CO molecules. In addition to the 1.4×1.4 phase in molecular resolution, the STM image shows strong contrast modulations, in particular a stripe patterning along \vec{b} . This modulation is best observed when looking at lower CO rows (blue color scale); we name them L (for lower). Two neighboring L rows are separated by either one or two higher CO rows. These regions are called S and D for single and double higher rows, respectively (see Figure 1B).

A height profile along the white arrow in Figure 1A is shown in Figure 1C. Clearly, the S and D rows are 15 pm higher than the L rows. Moreover, within the D rows, we frequently observe significant brighter spots (named “BS”) made of three or rarely four CO molecules. The height profile in Figure 1C reveals that the BS spots are 15 pm higher than the D rows. Approximately 10 BS features are shown in Figure 1A.

The periodicity of the CO monolayer was carefully analyzed by taking the fast Fourier transform (FFT) of the STM topographic images. Figure 2A shows the FFT image of Figure 1A. The six bright spots forming a hexagon correspond to the 1.4×1.4 CO lattice. On the basis of the direct hexagonal lattice vectors \vec{a} and \vec{b} in Figure 1A, we define the reciprocal lattice vectors \vec{k}_a^{CO} , \vec{k}_b^{CO} , and \vec{k}_c^{CO} in Figure 2A. The FFT image of the bare Cu(111) surface (Figure 2B) also shows six hexagonally symmetric spots (named \vec{k}_a^{Cu} , \vec{k}_b^{Cu} , and \vec{k}_c^{Cu}) in the same directions. To see the details of the periodicity in the CO monolayer stripe patterns, line profiles were taken along the

principal directions \vec{k}_a (black line), \vec{k}_b (blue line), and \vec{k}_c (red line) as depicted in Figure 2C. Main peaks are located around 25 nm^{-1} for all three profiles, while stronger subdomain peaks at 10 nm^{-1} are observed only in the \vec{k}_a direction. For bare Cu(111), we plotted the data as dotted lines in Figure 2C. To determine the lattice constant of the CO monolayer precisely and remove any systematic error due to the drift and imperfection of experimental piezo calibration, we take the ratios $R_i = \vec{k}_i^{\text{Cu}}/\vec{k}_i^{\text{CO}}$ ($i = a-c$) individually for \vec{k}_a (black), \vec{k}_b (blue), and \vec{k}_c (red). We obtain an R_a of 1.42 ($=35.0/24.6$), an R_b of 1.39 ($=34.6/24.9$), and an R_c of 1.41 ($=36.0/25.5$) with an error of ± 0.02 (see Figure 2C). These results are clear evidence that the observed CO monolayer has a 1.4×1.4 structure. To the best of our knowledge, the STM image in Figure 1A is the first real-space evidence of the 1.4×1.4 phase discovered by Pritchard et al. using LEED.¹⁸

It should be noted that the ratio $R = \vec{k}_a^{\text{Cu}}/\vec{k}_a^{\text{CO}}$ is slightly different in the three directions; in particular, $R_a/R_b = 1.02$. This means that the CO row distance in the \vec{k}_a direction (i.e., the distance between CO rows running along \vec{b}) is ~2% larger than in the \vec{k}_b direction. While this difference is hardly above the error bar, it is consistent with the fact that the stripe formation breaks the 3-fold symmetry and indicates that the CO molecules are a little more densely packed along the stripes than perpendicular to them.

Stripe Formation. The stripe pattern formation was further investigated by analyzing the FFT line profiles (Figure 2C). The line profile along \vec{k}_a^{CO} displays an intense subpeak at $9.97 \pm 0.13 \text{ nm}^{-1}$. The wavenumber ratio with respect to the main peak ($\vec{k}_a^{\text{CO}} = 24.60 \pm 0.10 \text{ nm}^{-1}$) is 0.405 ± 0.006 . This peak at $0.4\vec{k}_a^{\text{CO}}$ corresponds to a periodic intensity modulation with a wavelength of $1/0.4 = 2.5$ times the main wavelength λ_{CO} [CO row distance (see Figure 1A)]. Because the $0.4\vec{k}_a^{\text{CO}}$ subpeak is absent or much weaker in the other two directions, we expect one-dimensional patterning, i.e., the appearance of stripes perpendicular to \vec{k}_a^{CO} , in agreement with the real-space picture.

In Figure 1A, the distance between two L rows is either $2\lambda_{\text{CO}}$ or $3\lambda_{\text{CO}}$, corresponding to the LSL or LDL sequence, respectively. The occurrence of S and D is irregular; i.e., S and D rows are not always alternating (as in ...LSLDLSLD...). However, there are about as many D as S rows, and the average distance between L rows is $2.5\lambda_{\text{CO}}$, which explains the peak at 0.4 ($=1/2.5$) in the FFT line profile (see Figure 2C). Therefore, the dominant subpeaks at 0.4 correspond to (blue/green) stripe formation along the \vec{k}_a (or $2\vec{a} + \vec{b}$) direction in the real-space STM image. Note that if the CO overlayer was in a perfectly periodic, commensurate 1.4×1.4 superstructure on Cu, we would expect some modulation with a period of $5\lambda_{\text{CO}}$ [$=7 \lambda_{\text{Cu}}$ (see the inset in Figure 1A)] that would show up as a sharp peak at $0.2\vec{k}_a^{\text{CO}}$ in the FFT. The absence of a such a peak shows that the CO row sequence is nonperiodic, in agreement with the real-space image.

Hence, through FFT analysis, we could understand that the STM image in Figure 1A consists of three main components, namely, region I ($k \sim 25 \text{ nm}^{-1}$) (1.4×1.4 structure), region II ($k \sim 10 \text{ nm}^{-1}$) (stripe rows), and region III ($k \sim 0 \text{ nm}^{-1}$) (nonsymmetric patterns including the BS features). The inverse FFT of regions I–III, shown in Figure 2D, provides direct visual support for these assignments.

As mentioned above, the S and D rows are separated by L rows and alternate in a nonperiodic but not completely random way. The S/D sequence resembles the quasi-periodic “silver mean” sequence on Ag films discussed by Smith et

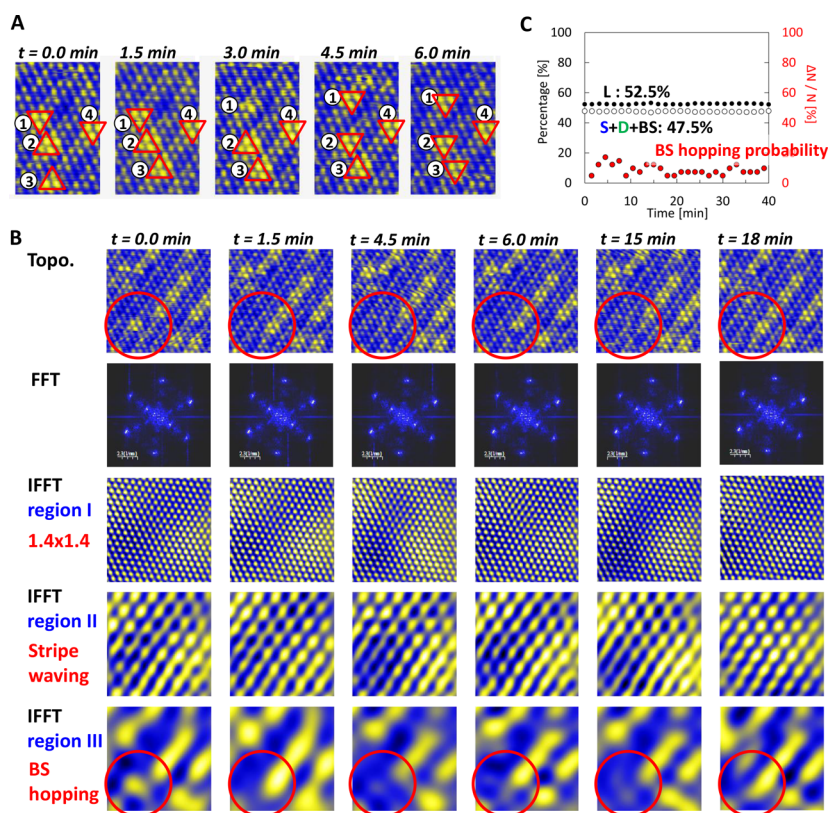


Figure 3. Time evolution of STM images at 4.6 K. (A) Successive STM topographic images obtained at the same area on the densely packed CO monolayer film on Cu(111). Each image was obtained with a 1.5 min interval. Four bright spots (BS) are marked by red triangles. (B) Time-dependent molecular hopping events. Six STM topographic images were obtained at 0.0, 1.5, 4.5, 6.0, 15, and 18 min. Corresponding FFT and IFFT images obtained using regions I–III in the FFT images are shown. (C) Time dependence of the coverage percentages for the lower (L, black dots) and higher (S, D, and BS, white dots) rows. The time dependence of the hopping probability (red circles) reveals approximately 9% of the CO molecules on the surface hop, where N and ΔN denote the total numbers of CO molecules in the STM image and numbers of hopping CO molecules in the STM image, respectively.

al.^{45–47} We find that the S/D sequence is consistent with the silver mean over a finite length of only ≤ 7 nm (see Figure S2 for details). While it is possible that the CO overlayer lattice has a quasi-crystal-like behavior of the silver mean type, we did not find enough experimental evidence to support this conclusion.

Correlated Molecular Hopping. We have studied the time evolution of the CO monolayer by taking successive STM images over a period of hours at a fixed temperature of 4.6 K under UHV. Interestingly, we found an apparent motion of the stripe pattern on a time scale of minutes. Such dynamic motion has not been reported before on any CO monolayer surface phase.

Figure 3A shows subsequent STM images of the same surface area taken at a time interval of 1.5 min, where four BS features (1–4) marked by red triangles are observed. From 0.0 to 1.5 min, feature 3 moved upward along the row direction. Then, from 1.5 to 4.5 min, feature 1 moved upward, and simultaneously, feature 2 changed the three spots upside down; no change was observed between 4.5 and 6.0 min. This type of CO molecular motion occurred continuously and randomly from one scan to the other on a time scale of minutes. The hopping events are clearly visible in the successive STM images [$t = 0.0$ –43.5 min (see Figures S3 and S4)] and videos (Videos 1–5).

To further investigate the lateral hopping event on the CO monolayer surface, we carefully checked the STM images in

the same area and corresponding FFT and the inverse FFT (IFFT) images produced with the FFT spots located in regions I–III. Figure 3B shows results at 0.0, 1.5, 4.5, 6.0, 15, and 18 min. We focus on the area marked by the circles in Figure 3B, where one BS feature hops from left to right between 0.0 and 1.5 min. Then, this BS repeatedly appeared and disappeared for 1.5–18 min. Between these events, the FFT, IFFT of region I (1.4×1.4 phase), and IFFT of region II (stripe waves) remain essentially unchanged, which means that the BS hopping dynamics does not affect the 1.4×1.4 phase or the stripe row periodicity. However, the IFFT of region III clearly shows the hopping events. The relative number of CO molecules in lower (L) and higher (S, D, and BS) rows is plotted in Figure 3C as a function of time. Although the hopping events occur frequently and at each time step, some 5% of the CO molecules switch between lower and higher sites, and the hopping does not change the statistical distribution of the molecules, which is very stable over 40 min: 52.5% in lower rows and 47.5% in higher rows (the latter being composed of 28.5% S, 12% D, and 7% BS).

These observations suggest that CO hopping is a stochastic process as expected for thermal or quantum fluctuations. We counted how many BS hopped every $\Delta t = 90$ s and normalized the hopping BS number (ΔN) by the total numbers of BS in the area (N). The hopping probability so obtained ($\Delta N/N$) is shown as red dots in Figure 3C, where the average indicates

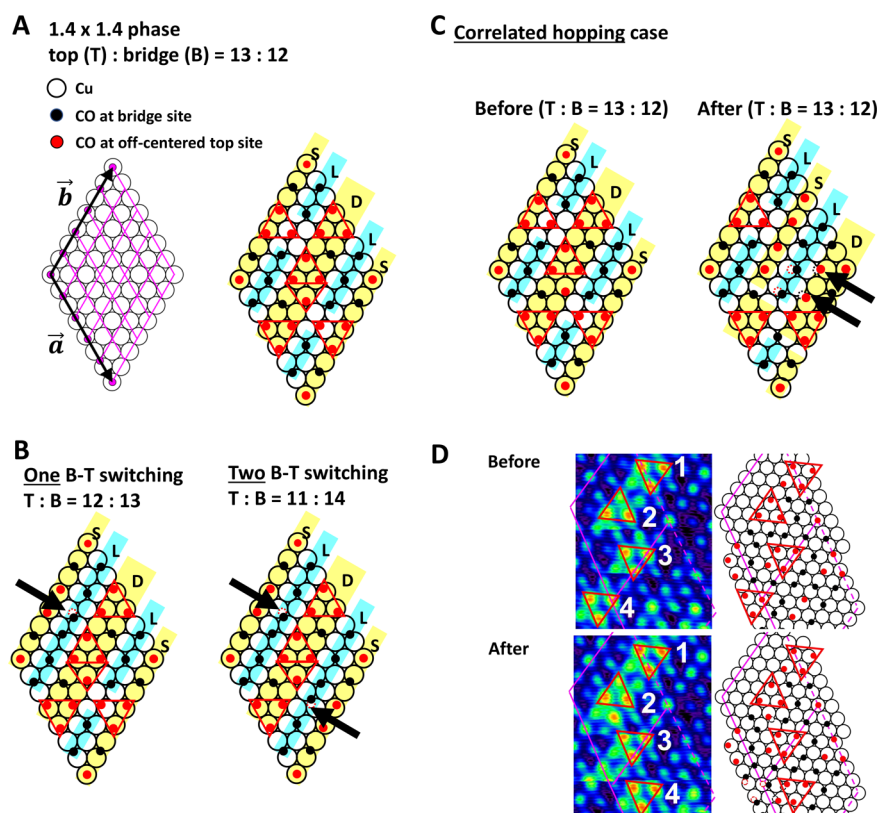


Figure 4. Models of the 1.4×1.4 CO phase on Cu(111). Black and white circles denote CO molecules and Cu atoms, respectively. (A) The left panel shows a coincidence lattice, with COs on perfect 1.4×1.4 lattice sites. The right panel shows 13 CO molecules located on the bridge sites and 12 CO molecules located on the off-center top sites. Yellow and blue regions denote higher and lower rows, respectively, reproducing the experimentally observed L, S, D, and BS. The BS are marked by red triangles. (B) Only one and two COs shift from off-center top to bridge sites, producing lower rows. Original CO positions are marked by dotted circles. (C) Models before and after the correlated hopping from top to bridge and bridge to top, maintaining the 13:12 ratio. (D) Models reproducing the experimentally obtained STM images before and after the correlated hopping.

8.9%. This yields a hopping rate = $(\Delta N/N)/\Delta t = 0.089/90 \text{ s}^{-1} \sim 1 \text{ mHz}$.

The hopping of CO on Cu(111) at temperatures of a few K is a complex phenomenon that may be caused by thermal diffusion, quantum mechanical tunneling, or tip effects. If the hopping were due to thermal diffusion alone, we could estimate the potential barrier from the measured hopping rate by Arrhenius' law. With a typical value for the attempt frequency of $10^{12} - 10^{13} \text{ s}^{-1}$, we obtain a barrier of $14 \pm 1 \text{ meV}$. However, this is much lower than the value of $\sim 100 \text{ meV}$ reported for single-CO diffusion at low coverage.²⁶ A possible reason for the discrepancy is that at the measurement temperature of 4.6 K, CO hopping is partially due to quantum tunneling. For small CO clusters on Cu(111), it was found that quantum tunneling dominates below 6 K.⁴ Finally, the hopping could be tip-induced. We did not see any evidence of strong tip effects such as a clear difference between STM images obtained in forward or backward scan directions (see Figure S7), while tiny scratches are observed, which may be tip-induced. The forward and backward scans show identical BS features. Nonetheless, the possibility that CO hopping is triggered either by the electric field between tip CO and surface CO³⁴ or by vibrational heating through inelastic electron scattering⁴⁸ cannot be fully ruled out.

Then the question arises why the 1.4×1.4 phase is easily seen in LEED, even at much higher temperatures (20–70 K). Contrary to STM, which measures the absolute atomic

positions on a time scale much slower than that of molecular motion (picosecond), LEED is a fast reciprocal-space probe and thus sensitive only to the instantaneous position of a scattering atom relative to its neighbors (i.e., it measures the pair correlation function). Consequently, the LEED pattern hardly changes when CO molecules hop from bridge to top sites, as long as the statistical distribution of the distance vectors between neighboring molecules is preserved, which is the case for collective CO hopping events observed in Figure 3.

Adsorption Models. We now discuss the molecular structure of the 1.4×1.4 phase of CO/Cu(111) in view of the models suggested previously by Pritchard.¹⁸ Figure 4A shows the schematic model of the 1.4×1.4 phase. The super cell unit contains $5 \times 5 = 25$ CO molecules and $7 \times 7 = 49$ Cu substrate atoms (circles). Using unit vectors of the substrate fcc(111) Cu lattice, $\vec{a}_{\text{Cu}} = \left(\frac{1}{2}, \frac{-\sqrt{3}}{2}\right)$ and $\vec{b}_{\text{Cu}} = \left(\frac{1}{2}, \frac{\sqrt{3}}{2}\right)$, the supercell unit vectors can be described as $\vec{a} = 7\vec{a}_{\text{Cu}} = 5\vec{a}_{\text{CO}}$ and $\vec{b} = 7\vec{b}_{\text{Cu}} = 5\vec{b}_{\text{CO}}$ (see Figure S6 for notation clarification). CO molecules adsorbed on off-center top (T) and bridge (B) sites are shown in Figure 4 as red and black dots, respectively.

We start with the coincidence structure, i.e., a regular 1.4×1.4 lattice of CO simply overlaid on the substrate lattice (see Figure 4A, left panel). This model contains top sites, off-center top sites, bridge sites, and a few hollow sites. A coincidence lattice is expected for a completely flat potential energy surface, but this is not realistic. According to Pritchard¹⁸ and Raval et

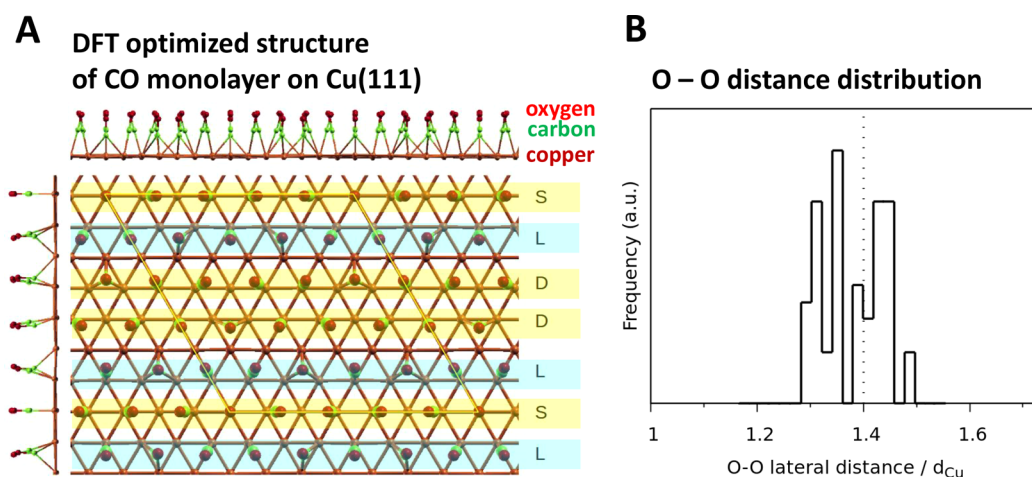


Figure 5. (A) Top view (center) of the calculated CO/Cu(111) structure. Oxygen (red), carbon (green), and surface layer copper atoms (brown) are shown. The 7×7 unit cell (dashed line) contains 25 CO molecules. CO rows attributed to higher (S and D) lines are shaded yellow, and lower (L) rows are shaded blue. (B) Histogram of the lateral O–O distance in the calculated CO/Cu(111) structure. It is seen that the O–O distances are narrowly distributed around $1.4d_{Cu}$, corresponding to a perfect 1.4×1.4 superstructure.

al.,²⁸ relaxation of the CO positions is crucial such that only top and 2-fold bridge sites are occupied with as many top sites as possible, because the top site is clearly preferred on Cu. The model suggested by Pritchard has a 13:12 ratio of top:bridge sites and is shown in Figure 4A (right panel). Note the appearance of groups of three or four molecules on adjacent off-center top sites (red dots). As seen in the right panel of Figure 4A, there are rows with only bridge sites (L, shaded blue) and rows with a majority of top sites (S or D, shaded yellow).

It was pointed out that the coincidence structure (Figure 4A, left panel) and the relaxed structure (Figure 4A, right panel) would be indistinguishable in LEED,²⁸ and to date, there has been no direct experimental evidence for either model. However, our STM data contain evidence favoring the relaxed model. In Figure 1A, there are bright (“BS”) features of three (sometimes four) CO molecules, which we attribute to CO on adjacent top sites. The apparent height of the BS molecules is ~ 15 pm larger than the other spots in single or double higher rows (see Figure 1C). For CO/Cu(100) in the $c(7\sqrt{2} \times \sqrt{2})$ phase, it was shown that CO molecules on nearest-neighbor top sites appear much brighter than CO molecules on next nearest-neighbor top sites.³⁰ The difference in apparent height was found to be 30 pm, in good agreement with the difference of 15 pm observed here. CO molecules on the nearest-neighbor Cu(001) top sites were shown to be strongly tilted,³³ which reduces the Pauli repulsion. The enhanced apparent height in STM images of the tilted molecules was attributed to an increase in O p_z and C p_z orbital character of the states around the Fermi level, which is the dominant tunneling channel in the case of a CO tip. The distance between the next nearest-neighbor sites on Cu(100) is $\sqrt{2}d_{Cu}$, which is only 1% larger than the distance between CO molecules in the 1.4×1.4 phase in CO/Cu(111). Thus, the effect of compression and adjacent site occupation should be quite comparable between the two systems. Our density functional theory (DFT) calculations (see Figure 5) show that also for CO/Cu(111), CO molecules adsorbed on the nearest-neighbor top sites are strongly tilted (by about 10°). Due to the triangular symmetry of Cu(111), three such molecules naturally form a

regular triangle, which explains the appearance of bright BS features.

Note that our experimental results are compatible with the hexagonal 1.4×1.4 model proposed by Pritchard, which also features five different rows per cell and clusters of three or four top atoms. However, we clearly observe a small, local breaking of the 3-fold symmetry by stripe formation. This does not contradict the observation of regular 1.4×1.4 LEED patterns, because the hexagonal lattice distortion is very small and in a LEED experiment the average over equivalent domains is seen.

An important new feature observed in this phase is the correlated switching between the top (T) and bridge (B) sites. Due to the repulsive intermolecular interaction of the CO overlayer, the rows where the CO molecules are closely arranged together would be more likely to switch adsorption site, which is the rows with top sites adjacent to each other.

In the left panel of Figure 4B, one of the top site CO marked by the arrow shifts to the near bridge site, and a row of bridge sites is formed (blue shade along the \mathbf{b} direction), corresponding to the experimentally observed lower row. This shift (from top to bridge) is portrayed by the dotted red circle. The right panel in Figure 4B represents another hopping model of two COs marked by arrows from top to bridge site. These models give us important insights into the stripe motion; namely, only one or two COs hopping between top and bridge sites control stripe formation.

Figure 4C depicts the situation before and after the correlated hopping. Two COs shift from top to bridge sites, and subsequently, two neighboring COs shift from bridge to top sites (see CO molecules marked by arrows). As a consequence, the bright BS feature located at the center of the model has vanished. Also, the original SLDLS rows switch to SLSLD rows. Collectively, the switching of adsorption sites results in stripe motion, which is the shifting of a D row to an S row.

Finally, Figure 4D shows models corresponding to the real hopping occurrence in the STM images. BS features 1–4 can be observed before the hopping, while feature 4 shifts the position after the hopping. The corresponding models suggest three COs shift from top to bridge sites and three COs shift from bridge to top sites.

Density Functional Theory Calculations. We have performed DFT calculations on the 1.4×1.4 monolayer phase of CO/Cu(111). Figure 5A shows the optimized structure of the 1.4×1.4 phase. Among the 25 CO molecules in the unit cell, 19 are adsorbed on top (T), three on bridge (B), and three on hollow (H) sites. However, only one of the top site COs is straight (T_s) on Cu, while 18 COs are tilted (T_t), most of them in the direction of a Cu–Cu bond, such that the x – y position of the O atom is between the top and bridge site. We now attribute the CO rows of the DFT calculation from top to bottom to the experimentally observed rows L, S, and D. Row 1 (top row in Figure 5, marked S) has the adsorption site sequence $T_s T_t T_t T_t T_t$. It contains only top sites and is attributed to the higher single row (S). Rows 3 ($T_t T_t T_t T_t H$) and 4 ($T_t B T_t T_t T_t$) are two adjacent rows with 80% tilted top sites and can be attributed to the higher double row (D). The remaining rows, 2 ($T_t B T_t B T_t$) and 5 ($T_t T_t H T_t H$), separate the single and double rows. They have the largest number (40%) of nontop sites. Moreover, the three top sites in each row are very strongly tilted such that the O atoms are closer to bridge sites than top sites. Considering the fact that the bridge site energy is overestimated in the present DFT+U scheme, we think that these three strongly tilted top site molecules might in reality be adsorbed on bridge sites. Therefore, we attribute rows 2 and 5 to the lower rows (L).

Figure 5B shows the statistical distribution of the lateral O–O distances in the optimized structure. Importantly, all lateral O–O distances are very close to the $1.4 \times$ Cu–Cu distance. Thus, the O positions alone form an almost perfect 1.4×1.4 structure. The tilting of the CO molecules clearly indicates that the O atoms of neighboring CO molecules repel each other. As adsorption at a top site has the lowest energy, the system tries to maximize the number of top sites, while keeping the O atoms as far apart as possible. This leads to a regular lattice of O positions and tilting of the CO top sites. It is important to note that the computed structure should appear as a very regular 1.4×1.4 superstructure in both STM and LEED, because these experiments essentially probe only the topmost atomic layer, i.e., the O positions.

In conclusion, the DFT simulations confirm the 1.4×1.4 superstructure and are consistent with the observation of single and double top site rows alternating with rows of mainly bridge sites.

Finally, we have analyzed the dI/dV curves of CO molecules in a lower and higher row (see Figure S5). We find that all lower row COs have a very similar dI/dV signal while approximately half of the higher row COs have a distinctly different signal. This corroborates the models in Figure 4 where the lower rows are adsorbed at a unique site (bridge) while the higher rows are a mixture of off-center top and bridge sites.

In summary, we have achieved the first real-space observation of the 1.4×1.4 phase of CO/Cu(111) using STM at 4.6 K. Locally, the hexagonal symmetry is broken by the formation of stripes between CO rows of different apparent heights. We distinguish three types of adsorption states, namely, lower (L) single CO rows, higher single (S) or double (D) rows, and bright spots (BS) made of three or four CO molecules, which appear randomly within the D rows. On the basis of DFT calculations, we assign the L rows to bridge adsorption sites, the S and D rows to a mixture of top and bridge sites, with a majority of off-center top sites, and the BS features to three nearest-neighbor, titled top site molecules. By

studying the time evolution of the STM images, we have observed an apparent motion of the stripe pattern that is explained by the correlated hopping of one to three CO molecules between adjacent top and bridge sites.

METHODS

Home-Built Low-Temperature UHV STM Setup. The experiment was performed with a home-built low-temperature STM instrument at 4.6 K under UHV. The setup consists of introduction, preparation, and analytical chambers with a base pressure of $<10^{-8}$ Pa (see details in refs 34–37). A UHV cryostat (CryoVac), including an outer liquid nitrogen tank (8 L) and an inner helium tank (4 L), is docked on the analytical chamber. The STM instrument was placed at the center of the analytical chamber thermally contacting the cryostat. Heat radiation from the analytical chamber to the STM instrument was cut with two cylindrical cooling shields, which maintained the STM temperature of 4.6 K for 40 h using 4 L of liquid helium.

STM/STS Measurements. STM and scanning tunneling spectroscopy (STS) measurements were performed with a combined Nanonis SPM controller and software. The topographic images were obtained with a constant current mode. STS was performed by measuring tunneling current as a function sample bias voltage [$I(V)$] at each pixel position in an STM topographic image (feedback off grid mode). Differential conductance (dI/dV) curves, which are proportional to the sample local density of states (LDOS), were obtained using WSxM 5.0 Develop 9.0 software³⁸ via numerical differentiation of $I(V)$ by the sample bias voltage (V).

Fabrication of the CO-Functionalized W Tip. STM tips were fabricated from polycrystalline W wires with a radius of 0.3 mm (99.95% pure) via electrochemical etching using aqueous KOH and subsequently transferred into the UHV preparation chamber. Then, the tip apex was flashed at 2000 K to exclude oxide layers.³⁹ The cleaned W tip was again transferred to the UHV analytical chamber without breaking UHV and placed in the STM instrument using a wobble stick. The W tip was approached on the Cu(111), and then CO gas was dosed. We prepared a CO-functionalized W tip by picking up an adsorbed CO single molecule from the Cu(111) surface on the W tip apex^{33,34} or direct adsorption of a CO gas molecule on the W tip apex.

Cu(111) Preparation. The Cu(111) single crystal was cleaned by repeated cycles of Ar⁺ sputtering (1.0 kV, 0.80 μ A) for 15–30 min with subsequent annealing (820 K) (see details in refs 34 and 37). The cleanliness of the substrate was checked using LEED. The cleaned Cu(111) was cooled first at the 100 K cooling stage for 15 min and second at the STM sample stage while the temperature of 4.6 K was maintained for at least 3 h. This avoided unnecessary thermal drift during approach and scanning. In most cases, immediately after the surface had been cleaned, atomically flat terraces (>100 nm) were produced with an impurity concentration of $<1\%$. dI/dV curves were measured to check the Cu(111) surface state peak at -0.35 eV below the Fermi energy.

CO Molecule Adsorption at Cryogenic Temperatures. The cleaned Cu(111) in the preparation chamber of the UHV-STM setup was subsequently transferred to the STM analytical chamber through the gate valve without breaking UHV. Then, we opened the two cooling shields cutting the radiation heat from the 300 K chambers and set the Cu(111) sample into the STM sample stage maintained at 5 K. We closed the shield

doors and waited 2–3 h to cool the sample to 5 K. We again opened the shield doors shortly (which heats the sample stage temperature from 5 to ~20 K) and gently dosed the CO gas molecules into the STM stage. CO gas was exposed to the STM chamber in an amount of 1.0 L (Langmuir, 1.33×10^{-6} mbar s) from the CO gas cylinder (0.9 MPa) through a variable leak valve. Then, the CO/Cu(111) sample was again allowed to cool, and after the temperature has stabilized at 4.6 K, STM measurement was carried out.

Density Functional Theory Calculations. Density functional theory (DFT) calculations were performed using the VASP code in the DFT+U scheme with the PBE exchange-correlation functional. Following ref 40, we took $U = 6$ eV for the 2p orbitals of C and O. A plane wave energy cutoff of 400 eV and a $2 \times 2 \times 1$ k -point mesh were used. The Cu(111) substrate was modeled with a four-atom layer slab in the 7×7 surface cell. The unit cell contains 196 Cu atoms and 25 CO molecules. Slabs were separated by 15 Å vacuum. The lower two Cu layers were frozen. The coordinates of all other atoms were optimized until the forces were < 0.1 eV/atom.

The CO/Cu system is a notorious case in which pure DFT functionals fail to predict the correct (top) adsorption site.⁴¹ Correlation effects beyond DFT need to be taken into account, by using configuration interaction,⁴² the random phase approximation,⁴³ or the computationally much less demanding DFT+U approach.^{40,41} Following Eran et al.,⁴⁰ we have chosen with the PBE+U functional a U value of 6 eV for the 2p orbitals of both C and O atoms. This functional predicts the top site to be most stable with an adsorption energy of -0.5 eV, in good agreement with experiment. It is generally believed that the hollow site is less stable than the bridge site,^{27,44} but the experimental evidence is rather limited and indirect, because hollow and bridge sites can be difficult to distinguish, e.g., in RAIRS.²⁷ Within the present PBE+U approach, we have $E(\text{top}) < E(\text{hollow}) < E(\text{bridge})$; i.e., the order of bridge and hollow sites appears to be reversed as compared to experiment.

■ ASSOCIATED CONTENT

SI Supporting Information

The Supporting Information is available free of charge at <https://pubs.acs.org/doi/10.1021/acs.jpcllett.9b03645>.

UHV STM topographic images obtained on the Cu(111) surface after dosing 0.1 and 0.5 L of CO (Langmuir) (Figure S1), discussion of the Silver mean sequence for the CO stripe row alignment (Figure S2), successive STM topographic images ($t = 0.0$ –43.5 min, time interval of 1.5 min per image) obtained on the 1.4×1.4 phase of CO/Cu(111) using STM at 4.6 K (Figure S3), successive inverse FFT images ($t = 0.0$ –43.5 min, time interval of 1.5 min per image) using the submain peaks in the FFT images, showing clearly the stripe pattern formation and dynamical wave motion, obtained on the 1.4×1.4 phase of CO/Cu(111) using STM at 4.6 K (Figure S4), STM spectroscopy dI/dV results obtained on the stripe rows in the 1.4×1.4 phase of CO/Cu(111) using STM at 4.6 K (Figure S5), schematic diagram depicting the Cu lattice unit vectors and the corresponding CO unit lattice (Figure S6), and STM images on the CO 1.4×1.4 phase when the STM tip scanned from left to right (forward) and right to left (backward) (Figure S7) (PDF)

Video 1 (MP4)

Video 2 (MP4)

Video 3 (MP4)

Video 4 (MP4)

Video 5 (MP4)

■ AUTHOR INFORMATION

Corresponding Author

Toyo Kazu Yamada – Department of Materials Science and Molecular Chirality Research Centre, Chiba University, Chiba 263-8522, Japan; orcid.org/0000-0001-5185-6472; Email: toyoyamada@faculty.chiba-u.jp

Authors

Nana K. M. Nazriq – Department of Materials Science, Chiba University, Chiba 263-8522, Japan

Peter Krüger – Department of Materials Science and Molecular Chirality Research Centre, Chiba University, Chiba 263-8522, Japan; orcid.org/0000-0002-1247-9886

Complete contact information is available at:

<https://pubs.acs.org/doi/10.1021/acs.jpcllett.9b03645>

Notes

The authors declare no competing financial interest.

■ ACKNOWLEDGMENTS

This work was supported by JSPS KAKENHI Grants 19H05789, 17K19023, 15K13357, 15H03531, 15H06092, 25110011, and 25600012 and the Murata Science Foundation. The authors thank Prof. Wolf Widdra for a fruitful discussion of the quasi-periodic silver mean and Mr. Tetsushi Yamada for assistance at an early stage of the DFT calculations.

■ REFERENCES

- (1) Lan, J.; Hutter, J.; Iannuzzi, M. First-Principles Simulations of an Aqueous CO/Pt(111) Interface. *J. Phys. Chem. C* **2018**, *122*, 24068–24076.
- (2) Zhang, K.; Li, L.; Shaikhutdinov, S.; Freund, H. J. Carbon Monoxide Oxidation on Metal-Supported Monolayer Oxide Films: Establishing Which Interface is Active. *Angew. Chem., Int. Ed.* **2018**, *57*, 1261–1265.
- (3) Liu, S.; Ishimoto, T.; Koyama, M. How Oxides Affect the Stretching Modes of Carbon Monoxide Adsorbed on Ni Catalyst. *Appl. Surf. Sci.* **2019**, *478*, 1074–1080.
- (4) Heinrich, A. J.; Lutz, C. P.; Gupta, J. A.; Eigler, D. M. Molecule cascades. *Science* **2002**, *298*, 1381–7.
- (5) Kuz'min, M. V.; Mittsev, M. A. Influence of CO Admolecules on the Electronic State of Ytterbium Nanofilms Grown on Silicon Substrates. *Tech. Phys.* **2019**, *64*, 1024–1028.
- (6) Gomes, K. K.; Mar, W.; Ko, W.; Guinea, F.; Manoharan, H. C. Designer Dirac Fermions and Topological Phases in Molecular Graphene. *Nature* **2012**, *483*, 306–310.
- (7) Kempkes, S. N.; Slot, M. R.; van den Broeke, J. J.; Capiod, P.; Benalcazar, W. A.; Vanmaekelbergh, D.; Bercieux, D.; Swart, I.; Morais Smith, C. Robust Zero-Energy Modes in an Electronic Higher-Order Topological Insulator. *Nat. Mater.* **2019**, *18*, 1292–1297.
- (8) Drost, R.; Ojanen, T.; Harju, A.; Liljeroth, P. Topological States in Engineered Atomic Lattices. *Nat. Phys.* **2017**, *13*, 668–671.
- (9) Collins, L. C.; Witte, T. G.; Silverman, R.; Green, D. B.; Gomes, K. K. Imaging Quasiperiodic Electronic States in a Synthetic Penrose Tiling. *Nat. Commun.* **2017**, *8*, 15961.
- (10) Slot, M. R.; Kempkes, S. N.; Knol, E. J.; Van Weerdenburg, W. M. J.; Van Den Broeke, J. J.; Wegner, D.; Vanmaekelbergh, D.; Khajetoorians, A. A.; Morais Smith, C.; Swart, I. P. Band Engineering in Artificial Electronic Lattices. *Phys. Rev. X* **2019**, *9*, 011009.

- (11) Leon, C. C.; Liu, Q.; Ceyer, S. T. CO Adsorption on Gold Nickel Au-Ni(111) Surface Alloys. *J. Phys. Chem. C* **2019**, *123*, 9041–9058.
- (12) Manzi, S.; Brites Helú, M. A.; Tysoe, W. T.; Calaza, F. C. Combining IR Spectroscopy and Monte Carlo Simulations to Identify CO Adsorption Sites on Bimetallic Alloys. *J. Phys. Chem. C* **2019**, *123*, 8406–8420.
- (13) Gunasooriya, G. T. K. K.; Saeys, M. CO Adsorption on Pt(111): From Isolated Molecules to Ordered High-Coverage Structures. *ACS Catal.* **2018**, *8*, 10225–10233.
- (14) López, Y. C. V.; Carrión, S. M.; López, M. B. Adsorption and Oxidation of Carbon Monoxide in a Sheet of β -Graphyne: Theoretical Study. *Rev. Mater.* **2018**, *23*, No. e12111.
- (15) You, H.; Fain, S. C. Structure of Carbon Monoxide Monolayers Physisorbed on Graphite. *Surf. Sci.* **1985**, *151*, 361–373.
- (16) Wu, H.; Ren, P.; Zhao, P.; Gong, Z.; Wen, X.; Cui, Y.; Fu, Q.; Bao, X. Dynamic Nanoscale Imaging of Enriched CO Adlayer on Pt(111) Confined under h-BN Monolayer in Ambient Pressure Atmospheres. *Nano Res.* **2019**, *12*, 85–90.
- (17) Hollins, P.; Pritchard, J. Interactions of CO Molecules Adsorbed on Cu(111). *Surf. Sci.* **1979**, *89*, 486–495.
- (18) Pritchard, J. On the Structure of CO Adlayers on Cu(100) and Cu(111). *Surf. Sci.* **1979**, *79*, 231–244.
- (19) Szabó, A.; Kiskinova, M.; Yates, J. T. Carbon Monoxide–Oxygen Interaction on the Pt(111) Surface: an Electron Stimulated Desorption Ion Angular Distribution (ESDIAD) Study. *J. Chem. Phys.* **1989**, *90*, 4604–4612.
- (20) Eve, J.; McCash, E. Low-Temperature Adsorption of CO on Cu(111) Studied by RAIRS. *Chem. Phys. Lett.* **2002**, *360*, 202–208.
- (21) Uvdal, P.; Karlsson, P.-A.; Nyberg, C.; Andersson, S.; Richardson, N. V. On the Structure of Dense CO Overlayers. *Surf. Sci.* **1988**, *202*, 167–182.
- (22) Ishi, S.; Ohno, Y.; Viswanathan, B. An Overview on the Electronic and Vibrational Properties of Adsorbed CO. *Surf. Sci.* **1985**, *161*, 349–372.
- (23) Eve, J.; McCash, E. Low-Temperature Adsorption of CO on Cu(111) Studied by Reflection Absorption Infrared Spectroscopy. *Chem. Phys. Lett.* **1999**, *313*, 575–581.
- (24) Ishi, S.; Ohno, Y.; Viswanathan, B. An Overview on the Electronic and Vibrational Properties of Adsorbed CO. *Surf. Sci.* **1985**, *161*, 349–372.
- (25) Hollins, P.; Pritchard, J. Interactions of CO Molecules Adsorbed on Cu(111). *Surf. Sci.* **1979**, *89*, 486–495.
- (26) Kole, P. R.; Hedgeland, H.; Jardine, A. P.; Allison, W.; Ellis, J.; Alexandrowicz, G. Probing the Non-Pairwise Interactions between CO Molecules Moving on a Cu(111) Surface. *J. Phys.: Condens. Matter* **2012**, *24*, 104016.
- (27) Hayden, B. E.; Kretzschmar, K.; Bradshaw, A. M. An Infrared Spectroscopic Study of CO on Cu(111): The Linear, Bridging and Physisorbed Species. *Surf. Sci.* **1985**, *155*, 553–566.
- (28) Raval, R.; Parker, S. F.; Pemble, M. E.; Hollins, P.; Pritchard, J.; Chesters, M. A. FT-RIRS, EELS and LEIS Studies of the Adsorption of Carbon Monoxide on Cu(111). *Surf. Sci.* **1988**, *203*, 353–377.
- (29) Tüshaus, M.; Berndt, W.; Conrad, H.; Bradshaw, A. M.; Persson, B. Understanding the Structure of High Coverage CO Adlayers. *Appl. Phys. A: Solids Surf.* **1990**, *51*, 91–98.
- (30) Persson, B. N. J.; Tüshaus, M.; Bradshaw, A. M. On the Nature of Dense CO Adlayers. *J. Chem. Phys.* **1990**, *92*, 5034–5046.
- (31) Bartels, L.; Meyer, G.; Rieder, K.-H. The Evolution of CO Adsorption on Cu(111) as Studied with Bare and CO-Functionalized Scanning Tunneling Tips. *Surf. Sci.* **1999**, *432*, L621–L626.
- (32) Biberian, J. P.; Van Hove, M. A. A New Model for CO Ordering at High Coverages on Low Index Metal Surfaces: a Correlation between LEED, HREELS and IRS: I. CO Adsorbed on fcc (100) Surfaces. *Surf. Sci.* **1982**, *118*, 443–464.
- (33) Thamankar, R.; Meyerheim, H. L.; Ernst, A.; Ostanin, S.; Maznichenko, I. V.; Soyka, E.; Mertig, I.; Kirschner, J. Tilting, Bending, and Nonterminal Sites in CO/Cu (001). *Phys. Rev. Lett.* **2011**, *106*, 106101.
- (34) Nazriq, N. K. M.; Minamitani, E.; Yamada, T. K. CO-Tip Manipulation Using Repulsive Interactions. *Nanotechnology* **2018**, *29*, 495701.
- (35) Inami, E.; Yamaguchi, M.; Yamaguchi, T.; Shimasaki, M.; Yamada, T. K. Controlled Deposition Number of Organic Molecules Using Quartz Crystal Microbalance Evaluated by Scanning Tunneling Microscopy Single-Molecule-Counting. *Anal. Chem.* **2018**, *90*, 8954–8959.
- (36) Inami, E.; Shimasaki, M.; Yorimitsu, H.; Yamada, T. K. Room Temperature Stable Film Formation of π -Conjugated Organic Molecules on 3d Magnetic Substrate. *Sci. Rep.* **2018**, *8*, 353.
- (37) Nemoto, R.; Kruger, P.; Putri Hartini, A. N.; Hosokai, T.; Horie, M.; Kera, S.; Yamada, T. K. Well-Ordered Monolayer Growth of Crown-Ether Ring Molecules on Cu(111) in Ultra-High Vacuum: An STM, UPS, and DFT Study. *J. Phys. Chem. C* **2019**, *123*, 18939–18950.
- (38) Horcas, I.; Fernández, R.; Gómez-Rodríguez, J. M.; Colchero, J.; Gómez-Herrero, J.; Baro, A. M. WSXM?: A Software for Scanning Probe Microscopy and a Tool for Nanotechnology. *Rev. Sci. Instrum.* **2007**, *78*, 013705.
- (39) Yamada, T. K.; Abe, T.; Nazriq, N. M. K.; Irisawa, T. Electron-Bombarded <110>-Oriented Tungsten Tips for Stable Tunneling Electron Emission. *Rev. Sci. Instrum.* **2016**, *87*, 033703.
- (40) Eren, B.; Zherebetskyy, D.; Patera, L. L.; Wu, C. H.; Bluhm, H.; Africh, C.; Wang, L. W.; Somorjai, G. A.; Salmeron, M. Activation of Cu(111) Surface by Decomposition into Nanoclusters Driven by CO Adsorption. *Science* **2016**, *351*, 475–478.
- (41) Gajdoš, M.; Hafner, J. CO Adsorption on Cu(111) and Cu(001) Surfaces: Improving Site Preference in DFT Calculations. *Surf. Sci.* **2005**, *590*, 117–126.
- (42) Sharifzadeh, S.; Huang, P.; Carter, E. Embedded Configuration Interaction Description of CO on Cu(111): Resolution of the Site Preference Conundrum. *J. Phys. Chem. C* **2008**, *112*, 4649–4657.
- (43) Ren, X.; Rinke, P.; Scheffler, M. Exploring the Random Phase Approximation: Application to CO Adsorbed on Cu(111). *Phys. Rev. B: Condens. Matter Mater. Phys.* **2009**, *80*, 045402.
- (44) Kole, P. R.; Hedgeland, H.; Jardine, A. P.; Allison, W.; Ellis, J.; Alexandrowicz, G. Probing the Non-Pairwise Interactions between CO Molecules Moving on a Cu(111) Surface. *J. Phys.: Condens. Matter* **2012**, *24*, 104016.
- (45) Smith, A. R.; Chao, K.-J.; Niu, Q.; Shih, C.-K. Formation of Atomically Flat Silver Films on GaAs with a Silver Mean Quasi Periodicity. *Science* **1996**, *273*, 226–8.
- (46) Ali, M. K.; Gumbs, G. Quasiperiodic Dynamics for a Generalized Third-Order Fibonacci Series. *Phys. Rev. B: Condens. Matter Mater. Phys.* **1988**, *38*, 7091–7093.
- (47) Gumbs, G.; Ali, M. K. Dynamical Maps, Cantor Spectra, and Localization for Fibonacci and Related Quasiperiodic Lattices. *Phys. Rev. Lett.* **1988**, *60*, 1081–1084.
- (48) Stroschio, J. A.; Celotta, R. J. Controlling the Dynamics of a Single Atom in Lateral Atom Manipulation. *Science* **2004**, *306*, 242–247.